Journal of Integrative Neuroscience, Vol. 5, No. 4 (2006) 561–593

Imperial College Press
www.icpress.co.uk

**Research Report**

# GENERATION OF THE RECEPTIVE FIELDS OF SUBPIAL CELLS IN TURTLE VISUAL CORTEX

WENXUE WANG[*,‡], SEAN LUO[†,§], BIJOY K. GHOSH[*,¶]
and PHILIP S. ULINSKI[†,**]

[*]*Department of Electrical and Systems Engineering*
*Washington University*
*Campus Box 1127, Bryan Hall 201*
*One Brookings Dr.*
*Saint Louis, MO 63130*

[†]*Committee on Computational Neuroscience*
*The University of Chicago*
*1025 E. 57th Street*
*Chicago, IL 60637*
[‡]*ww1@ese.wustl.edu*
[§]*xsl2101@columbia.edu*
[¶]*ghosh@netra.wustl.edu*
[**]*pulinski@uchicago.edu*

Received 15 September 2006
Accepted 14 November 2006

The visual cortex of turtles contains cells with at least two different receptive field properties. Superficial units are located immediately below the pial surface. They fire in response to moving bars located anywhere in binocular visual space and to two spots of light presented with different spatiotemporal separations. Their location in the cortex suggests that superficial units correspond to a distinct class of inhibitory interneurons, the subpial cells, that are embedded in geniculocortical axons as they cross the visual cortex of turtles. This study used a detailed compartmental model of a subpial cell and a large-scale model of visual cortex to examine the cellular mechanisms that underlie the formation of superficial units on the assumption that they are subpial cells. Simulations with the detailed model indicated that the biophysical properties of subpial cells allow them to respond strongly to activation by geniculate inputs, but the presence of dendritic beads on the subpial cells decreases their sensitivity and allows them to integrate the inputs from many geniculate afferents. Simulations with the large-scale model indicated that the responses of subpial cells to simulated visual stimuli consist of two phases. A fast phase is mediated by direct geniculate inputs. A slow phase is mediated by recurrent excitation from pyramidal cells.

[‡]Corresponding author.

It appears that subpial cells play a major role in controlling the information content of visual responses.

*Keywords*: Inhibitory interneurons; dendritic beads.

## 1. Introduction

Freshwater turtles have a visual cortex that contains cells that respond robustly to apparent motion and real moving stimuli [35]. Mazurskaya [21] studied their receptive field properties using extracellular recording methods in alert turtles and found two groups of neurons with different receptive field properties. Deep units were located between 800 $\mu$m and 1000 $\mu$m from the cortical surface and responded to moving bars located throughout the visual field. The best responses were obtained with bars moving with speeds of 5°/sec to 8°/sec. The direction of the moving bar did not significantly affect the firing rate of the cells. Deep units did not respond to two spots presented at disjunct points in visual space with some temporal separation, $\Delta t$. Plots of the number of action potentials produced by two spots of light as a function of $\Delta t$ showed two broad peaks, one in the range of $\Delta t = 50$ ms to $\Delta t = 200$ ms and a second in the range of $\Delta t = 500$ ms to $\Delta t = 1000$ ms. The positions of the two peaks shifted as a function of the spatial separation of the two spots, indicating that deep units have spatiotemporally inseparable receptive fields and could play a role in global motion detection [35]. Superficial units were located between 200 $\mu$m and 300 $\mu$m from the pial surface [21]. Like deep units, they had broad receptive fields, but were sensitive to turning lights on or off and appeared to fire for several hundred milliseconds following stimulus presentation. They also responded strongly to simultaneous presentation of two spots at different points in visual space. The firing profiles of the neurons showed three peaks that varied as a function of $\Delta t$. The first peak occurred with very short latency following presentation of the first spot. The second occurred in the range of $\Delta t = 10$ ms–100 ms, and the third peak occurred in the range of $\Delta t = 100$ ms–700 ms. In contrast to deep units, there was no statistically significant shift in the peaks as a function of spatial separation.

The relationship of deep and superficial units to the several anatomically distinct groups of cells present in turtle visual cortex (e.g., [6, 7, 9]) is not certain. However, reasonable inferences about their identity can be made based on their laminar positions in the cortex. Deep units have depths measured from the pial surface of the brain that correspond to the pyramidal cells that are the dominant population of cells in the intermediate layer 2 of the cortex [7]. The laminar positions of the superficial units correspond to the distribution of a distinctive group of inhibitory interneurons, the subpial cells, that are located in the outer half of layer 1 of the cortex [6]. Since no other type of cell is known to occupy this position in the visual cortex, it is likely that superficial units correspond to subpial cells. Subpial cells were first described in Golgi preparations by Desan [9]. It appears they are interneurons because they have local axonal arbors that extend principally throughout the outer half of layer 1 [6], and are not retrogradely labeled following injections of horseradish peroxidase in the brainstem [34]. Like several other populations of neurons in turtle

visual cortex [2, 28], subpial cells show antiGABA-like immunoreactivity and are presumed to be inhibitory. As their name indicates, subpial cells are positioned just below the pial surface [6] and are embedded in the fascicle of geniculate afferents that run across the visual cortex in turtles [13, 22]. Their dendrites are unusual in that they bear a large number of distinct beads or varicosities that account for roughly 70% of the total surface area of these cells [6]. Subpial cells show a marked spike rate adaptation in response to intracellular current injections, differing in this regard from other inhibitory neurons, such as stellate and horizontal cells, that show a fast spiking firing pattern with little spike rate adaptation [6, 16, 19].

The cellular mechanisms that underlie the receptive field properties of Mazurskaya's superficial units are unknown and involve several issues. First, subpial cells have dendritic fields that span only a fraction of the total length and width of the visual cortex and intersect geniculate afferents carrying information from a broad, but still restricted domain in visual space. It is, consequently, not known how the whole-field receptive fields of superficial units are generated. Second, it is not understood precisely why superficial units have a short latency and robust response to geniculate activation while deep units do not respond in that way. Third, the mechanisms underlying the generation of the intermediate and late peaks in the response profiles of superficial units are not known. Finally, the significance of the beads that occupy the major fraction of the surface area of subpial cells is not known.

This paper uses two biophysically realistic models to study the generation of their receptive field properties on the assumption that superficial units are subpial cells. The first is a detailed model of a subpial cell that is used to characterize the integration of multiple geniculate inputs by subpial cells. The second model is a large-scale model of the visual cortex that includes subpial cells represented by reduced compartmental models. This model was used to simulate the responses of subpial cells to diffused light flashes, spots of light presented with varying spatial and temporal separations, and to moving spots.

## 2. Methods

### 2.1. *Anatomy and physiology*

Subpial cells were filled with *Neurobiotin* following physiological analysis. Details were provided by Colombe *et al.* [6]. In brief, whole-cell recordings were made from subpial cells in coronal slices through the visual cortex using differential interference contrast optics. Voltage responses to 1 s square current pulses were recorded using an Axoclamp 2A preamplifier in bridge balance mode (Axon Instruments). They were used to characterize the voltage-current properties, firing patterns and spike morphologies of each cell. Slices containing *Neurobiotin*-injected neurons were fixed overnight, processed using avidin-biotin-horseradish peroxidase complex and reacted with diaminobenzidine. A confocal microscope was used to prepare a sketch of the cell selected for compartmental modeling in which the position of each bead and

each interbead segment was recorded. The diameters and lengths of the beads and segments were measured to the nearest 0.1 $\mu$m and entered on the drawing. Lengths, widths and surface areas of beads and interbead segments were collected using LSM 510 software (Zeiss).

Cell 3-12-99 was judged to be the best-filled subpial cell in the sample of 12 cells studied by Colombe *et al.* [7] and was used to construct the full and reduced compartmental models. The cell was situated 134 $\mu$m medial to the junction of the anterior dorsal ventricular ridge and the cortex, near the border of the medial and lateral parts of cortical area D. Its soma was situated 66 $\mu$m from the pial surface. Cells in the total sample had depths from the pial surface that ranged from 26 $\mu$m to 120 $\mu$m. The dendritic tree of cell 3-12-99 had a height of 113 $\mu$m and a width of 206 $\mu$m. The heights of the dendritic fields of cells in the total sample varied from 60 $\mu$m to 260 $\mu$m. The widths of the dendritic fields of cells in the total sample varied from 205 $\mu$m to 520 $\mu$m. Cell 3-12-99 had six primary dendrites which are labeled A through F in Fig. 1. The dendrites were apparently contained within the thickness of the section. Only two cells in the total sample were sufficiently complete to warrant detailed quantitative analysis of their dendritic trees. The dendrites of cell 3-12-99 had 138 beads, which occupied 73.2% of the total surface area of the cell, and 84 interbead segments, which occupied 17.9% of the total surface area of the cell. The other cell had 139 beads, which occupied 56.2% of its surface area, and 85 interbead segments, which occupied 12.3% of its surface area. The soma of cell 3-2-99 was approximately ellipsoidal in shape with a surface area that occupied

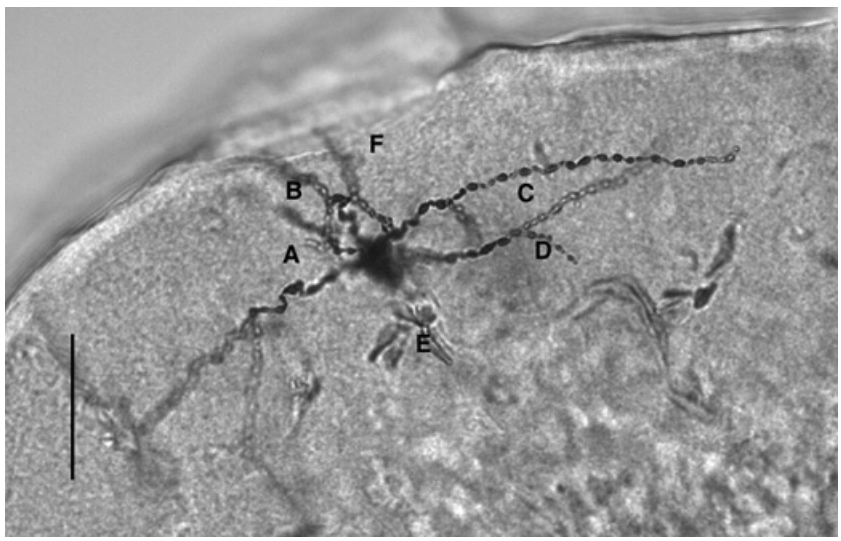


Fig. 1. Morphology of cell 3-12-99. This is a confocal micrograph of cell 3-12-99. The primary dendrites are labeled A through F. The pial surface is the arc across the top of the figure. Pyramidal cells in layer 2 of the cortex are visible at the lower right edge of the image. The lateral edge of the cortex is to the right. Thus, geniculate afferents enter the image from the left and proceed in an arc across the image. The vertical scale represents 50 $\mu$m.

8.9% of the cell's total surface area of 5419.3 $\mu$m$^2$. The other cell had a soma that occupied 31.5% of its total surface area of 5990.1 $\mu$m$^2$. The axon of cell 3-12-99 originated from the soma of the cell and could be traced a short distance to the surface of the section. Cell 3-12-99 cell had a measured total input resistance of 1.3 G$\Omega$ and a calculated specific membrane resistance of $R_m = 70\,\mathrm{k}\Omega\,\mathrm{cm}^2$. Total input resistances in the total sample of 12 cells ranged from 0.179 G$\Omega$ to 2.0 G$\Omega$. The membrane time constant of cell 3-12-99 was $\tau_0 = 31.5$ ms; the first equalizing time constant was $\tau_1 = 1.2$ ms. Time constants could be measured for 11 cells in the total sample. Values for the membrane time constant ranged from 21.6 ms to 89.4 ms. Values for the first equalizing time constant ranged from 1.4 ms to 2.3 ms. Values for the electrotonic length ranged from 0.5 to 2.1. Figure 2A shows the responses of the cell to depolarizing and hyperpolarizing current pulses. Increasing the amplitudes of depolarizing pulses resulted in decreased latencies to the first spike and increased numbers of spikes. Responses to +0.02 and +0.03 nA current pulses showed a distinct spike rate adaptation. This is quantified in Fig. 2B which is a plot of the instantaneous firing frequency of the cell as a function of time in response to a +0.03 nA current pulse. Responses to hyperpolarizing pulses showed a distinct inward rectification. This is illustrated in Fig. 2C, which is a plot of the voltage change produced by hyperpolarizing current pulses. Hyperpolarizing current pulses frequently produced off-depolarizations that could generate action potentials (Fig. 2A, −0.07 nA).

### 2.2. *Full compartmental model*

Each of the 138 beads and each of the 84 interbead segments in cell 3-12-99 was represented as a separate compartment. The surface area of each component of the cell was estimated by modeling beads as ellipsoids and interbead segments as cylinders. The soma was modeled as an ellipsoid. Figure 3A is a sketch of the full compartmental model. A second version of the model was constructed by replacing each of the beads by a cylinder with a length equal to the length of the bead and a diameter equal to the average diameter of the two neighboring interbead segments. This had the effect of converting the neuron with beaded dendrites into a neuron with smooth dendrites (Fig. 3B).

Each compartment was represented by an ordinary differential equation (see Bower and Beeman [5]):

$$\frac{dV_i(t)}{dt} = -\frac{1}{C_i}\left[\frac{(V_i(t) - E_r)}{R_i} + \sum_j \frac{[V_i(t) - V_j(t)]}{R_{ij}} + \sum_{ion} g_k(V_i(t) - E_k) + \sum_{syn} g_k(V_i(t) - E_k) + I_{stim}(t)\right] \tag{2.1}$$

where $V_i(t)$ is the time dependent membrane potential of the $i$th compartment relative to the resting membrane potential, $C_i$ is the total membrane capacitance of

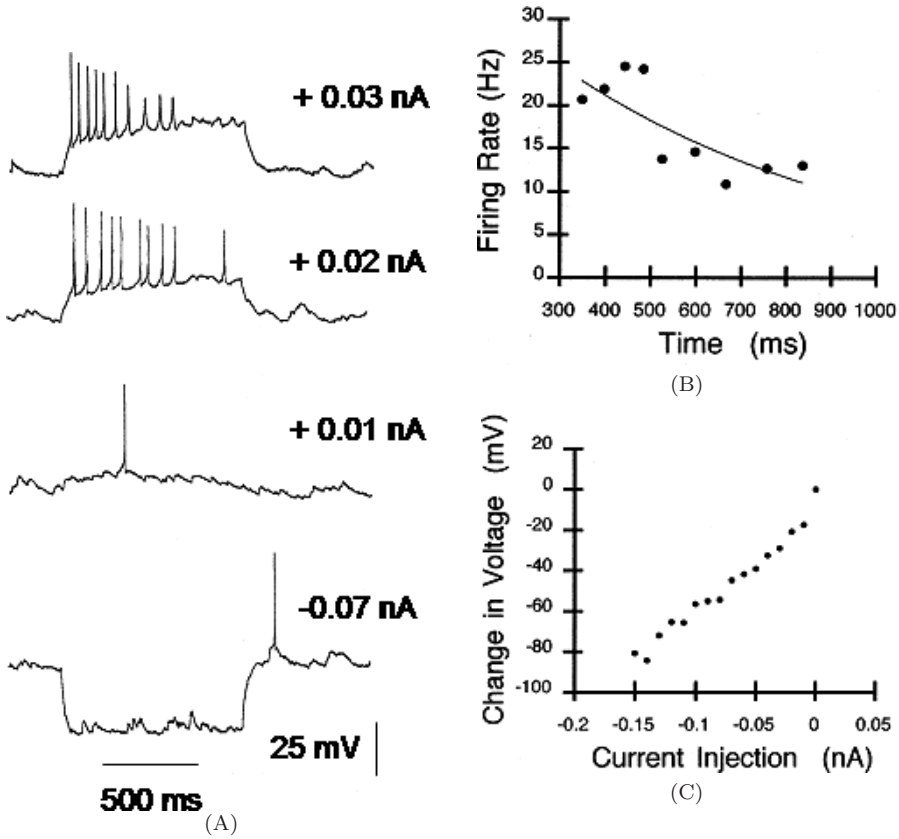


Fig. 2. Responses of cell 3-12-99 to intrasomatic current pulses. (A) Responses of the cell 3-12-99 to 1 s current pulses with amplitudes of +0.01 nA, +0.02 nA, +0.03 nA and −0.07 nA. (B) Firing rate adaptation curve. The instantaneous firing rate of cell 3-12-99 is plotted as a function of time after the onset of the current pulse, which took place at 300 ms. (C) Voltage-current plot for cell 3-12-99. The amplitudes of voltage deflections produced by hyperpolarizing current pulses are plotted as a function of the amplitudes of the current pulses.

the $i$th compartment, $R_i$ is the total membrane resistance of the $i$th compartment, and $R_{ij}$ is the coupling resistance between the $i$th and $j$th compartments. Total resistance and capacitance were calculated from the geometry of the compartments and the biophysical parameters: $R_m$, $C_m$ and $R_a$, using standard relationships [5]. The first summation in Eq. (2.1) is the over all compartments linked to the $i$th compartment. The second summation is the over all species of ionic conductances present on the $i$th compartment. The third summation is the over all species of synaptic conductances present on the $i$th compartment. $I_{stim}(t)$ is a square current pulse of 1 duration that was included in the soma compartment.

The response of the real cell (Fig. 4B, beads intact, noisy trace) to a −0.01 nA current pulse (Fig. 4A) was used to constrain the biophysical parameters of the full compartmental model with beads intact. Parameter values were: $R_m = 55\,\mathrm{k}\Omega\,\mathrm{cm}^2$, $C_m = 0.6\,\mu\mathrm{F/cm}^2$ and $R_a = 68\,\Omega\,\mathrm{cm}$. The same parameters were used for all of the

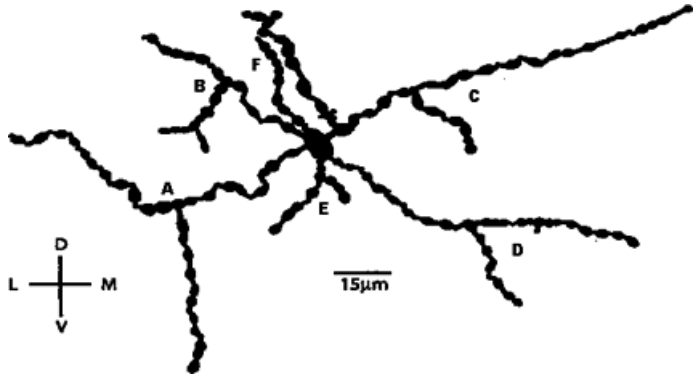


(A)


(B)

Fig. 3. Structure of compartmental models. This figure illustrates the morphological structure used for full and reduced compartmental models used in this study. (A) Structure of the full compartmental model. The soma and each varicosity and intervaricose segment are included. The primary dendrites are labeled A through F. Compare this drawing to the confocal image in Fig. 1. (B) Structure of the reduced compartmental model. Individual compartments are numbered.

compartments. Figure 4B compares the response of the real cell (beads intact, noisy trace) to the response of the full compartmental model (beads intact, smooth trace) to −0.01 nA intrasomatic current injections. The response of the model with beads intact closely follows the voltage response of the real cell, with the exception of a small off-depolarization that is present in the real cell but not in the model. The off-depolarization is likely due to an active conductance that is present in the real cell but not in the model cell.

### 2.3. *Reduced compartmental model*

A reduced compartmental model of cell 3-12-99 (Fig. 5) was obtained by reducing the 223 compartments in the full compartmental model to 29 using the method outlined by Stratford *et al.* [33]. In brief, the number of compartments was reduced in three steps. First, sequences of compartments in unbranched dendritic segments

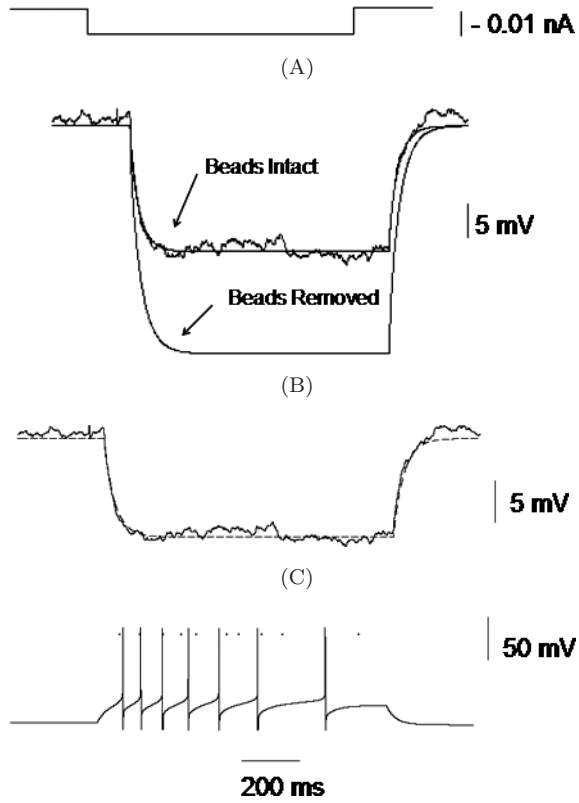


Fig. 4. Biophysical characteristics of compartmental models. This figure illustrates the responses of cell 3-12-99 and the full and reduced compartmental models to intrasomatic current pulses. (A) A −0.01 nA, 1 s current pulse. (B) The response of cell 3-12-99 to the −0.01 nA current pulse superimposed on the response of the passive model with beads intact in the upper two traces. The lower trace shows the response of the passive model with beads removed. (C) The response of cell 3-12-99 to a −0.01 nA current pulse superimposed on the response of the reduced compartmental model. (D) The response of the reduced compartmental model to a +0.02 nA current pulse. The occurrence times of spikes in cell 3-12-99 to a +0.02 nA current pulse are shown by dots.

were combined into single, cylindrical compartments. The length of the cylindrical compartment was obtained by dividing the total surface area of the contributing compartments by the diameter of the narrowest contributing compartment. Second, compartments involved in branched elements of the dendritic tree were combined. The diameter and length of each parent compartment were not changed. The lengths of daughter segments were normalized by $l'_i = l_i\sqrt{d_r/d_i}$ where $l_i$ is the length of the $i$th dendritic segment, $d_i$ is its diameter, $d_r$ is the diameter of the parent compartment, and $l'_i$ is the normalized length. The diameter of the combined daughter compartment is given by $d_c = (\sum_{i=1}^{n} d_i^{3/2})^{2/3}$ where $d_c$ is the diameter of the combined compartment, $n$ is the number of daughter compartments, and $d_i$ is the diameter of the $i$th daughter compartment. The length of the combined compartment is

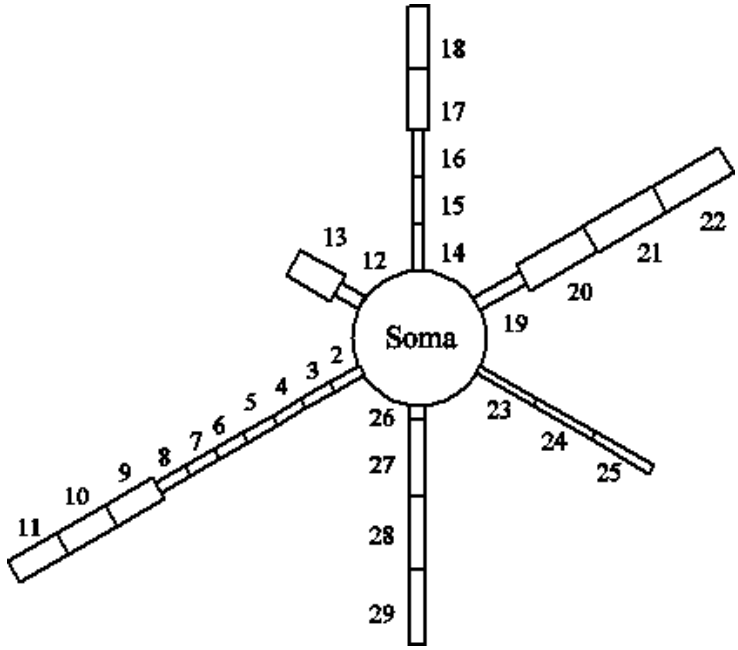


Fig. 5. Structure of the reduced compartmental model. Each soma and dendritic compartment in the reduced model is numbered.

$l_c = l_s\sqrt{d_c/d_r}$ where $l_s = \left(\sum_{i=1}^{n} l_i'\right)/n$. Third, compartments that were still relatively long were divided into three to four cylindrical compartments. Figure 3B shows the structure of the reduced compartmental model and the dendritic compartments were numbered from 2 through 29. The dimensions of each compartment are given in Table 1. Figure 4C compares the responses of the real cell and the reduced compartmental model to intracellular current pulses. The biophysical parameters of the model cell were constrained by varying the parameters in the model until the simulated response to a $-0.01\,\mathrm{nA}$ current pulse matched the response of the real cell to a current pulse of the same amplitude. The specific membrane resistance was $R_m = 34.7\,\mathrm{k\Omega\,cm^2}$. The specific membrane capacitance was $C_m = 0.4\,\mu\mathrm{F/cm^2}$. The axial resistance was $R_a = 285.6\,\Omega\,\mathrm{cm}$. The resting membrane potential of the cell was $V_r = -74.0\,\mathrm{mV}$.

### 2.4. *Active conductances*

Three voltage-gated currents and one calcium dependent current were included in the soma compartments of the full and reduced compartmental models. Unpublished experiments in our laboratory confirm that subpial cells have a tetrodotoxin sensitive fast sodium current and a tetraethylammonium sensitive delayed rectifier potassium current that underlie action potentials, but the kinetics of these conductances have not been characterized. Thus, a fast sodium ($I_{\mathrm{Na}}(V,t)$) and a delayed rectifier potassium ($I_{\mathrm{DR}}(V,t)$) current were specified by Hodgkin-Huxley equations

Table 1. Dimensions of compartments in reduced subpial cell model.

| Compartment | Diameter | Length | E_length | Connections |
|---|---|---|---|---|
| Soma | 9.5 $\mu$m | | | |
| Dend2 | 0.13 $\mu$m | 37 $\mu$m | 0.19 | To soma |
| Dend3 | 0.13 $\mu$m | 37 $\mu$m | 0.19 | To dend2 |
| Dend4 | 0.13 $\mu$m | 37 $\mu$m | 0.19 | To dend3 |
| Dend5 | 0.13 $\mu$m | 37 $\mu$m | 0.19 | To dend4 |
| Dend6 | 0.13 $\mu$m | 37 $\mu$m | 0.19 | To dend5 |
| Dend7 | 0.13 $\mu$m | 37 $\mu$m | 0.19 | To dend6 |
| Dend8 | 0.13 $\mu$m | 37 $\mu$m | 0.19 | To dend7 |
| Dend9 | 0.31 $\mu$m | 57 $\mu$m | 0.19 | To dend8 |
| Dend10 | 0.31 $\mu$m | 57 $\mu$m | 0.19 | To dend9 |
| Dend11 | 0.31 $\mu$m | 57 $\mu$m | 0.19 | To dend10 |
| Dend12 | 1.46 $\mu$m | 13 $\mu$m | 0.02 | To soma |
| Dend13 | 1.65 $\mu$m | 54 $\mu$m | 0.08 | To dend12 |
| Dend14 | 0.57 $\mu$m | 57 $\mu$m | 0.14 | To soma |
| Dend15 | 0.57 $\mu$m | 57 $\mu$m | 0.14 | To dend14 |
| Dend16 | 0.57 $\mu$m | 57 $\mu$m | 0.14 | To dend15 |
| Dend17 | 0.69 $\mu$m | 70 $\mu$m | 0.15 | To dend16 |
| Dend18 | 0.69 $\mu$m | 70 $\mu$m | 0.15 | To dend17 |
| Dend19 | 0.46 $\mu$m | 52 $\mu$m | 0.14 | To soma |
| Dend20 | 1.15 $\mu$m | 95 $\mu$m | 0.16 | To dend19 |
| Dend21 | 1.15 $\mu$m | 95 $\mu$m | 0.16 | To dend20 |
| Dend22 | 1.15 $\mu$m | 95 $\mu$m | 0.16 | To dend21 |
| Dend23 | 0.36 $\mu$m | 59 $\mu$m | 0.18 | To soma |
| Dend24 | 0.36 $\mu$m | 59 $\mu$m | 0.18 | To dend23 |
| Dend25 | 0.36 $\mu$m | 59 $\mu$m | 0.18 | To dend24 |
| Dend26 | 0.95 $\mu$m | 6 $\mu$m | 0.01 | To soma |
| Dend27 | 0.95 $\mu$m | 89 $\mu$m | 0.17 | To dend26 |
| Dend28 | 0.95 $\mu$m | 89 $\mu$m | 0.17 | To dend27 |
| Dend29 | 0.95 $\mu$m | 89 $\mu$m | 0.1667 | To dend28 |

(see Nenadic *et al.* [24]), modified from the model of a CA3 pyramidal cell in rat hippocampus. Parameters in the equations for these two currents were constrained by the latency, height, and width of the first action potential produced by intrasomatic injections of depolarizing currents in the model cells.

The ionic mechanisms underlying spike rate adaptation in subpial cells have not been fully characterized, but unpublished experiments in our laboratory show that subpial cells have a cadmium sensitive, high voltage calcium conductance that is visible when sodium spikes are blocked. Thus, a high voltage calcium current ($I_{\mathrm{Ca}}{}^{2+}(V,t)$) and a mAHP current ($I_{\mathrm{AHP}}([\mathrm{Ca}^{2+}],t)$, were used to produce spike rate adaptation in the model cell. The high voltage calcium current is a voltage dependent current, but the AHP current depends only on the intracellular calcium concentration, $[\mathrm{Ca}^{2+}]$. The maximal values of each conductance were constrained by comparing the simulated response of the model cell to depolarizing current pulses to the voltage responses of the real cell. Figure 4D shows the voltage trace produced in the reduced compartmental model cell by a +0.02 nA intrasomatic current pulse.

The dots represent the occurrence times of action potentials in the real cell. The model accurately represents the latencies of the first few spikes produced in the real cell and, like the real cell, shows a distinct spike rate adaptation. However, it was not possible to match every feature of the simulated spike train to spike trains elicited in real cells. In particular, the real cell shows a plateau potential that lasts for the duration of the current injection and leads to the generation of action potentials not seen in the model cell. These are likely due to the presence of voltage gated calcium or sodium channels or calcium buffering mechanisms that have not been characterized and were not incorporated in the model. The kinetic schemes used to specify voltage gated conductances and calcium fluxes are given by Nenadic *et al.* [24]. The maximal conductances used in the full compartment model are: $\overline{g}_{\mathrm{Na}^+} = 370\,\mathrm{mS/cm^2}$; $\overline{g}_{\mathrm{K}^+} = 250\,\mathrm{mS/cm^2}$; $\overline{g}_{\mathrm{K}^+_{\mathrm{AHP}}} = 0.02\,\mathrm{mS/cm^2}$; $\overline{g}_{\mathrm{Ca}^{2+}} = 2.3\,\mathrm{mS/cm^2}$. The maximal conductances used in the reduced compartment model are: $\overline{g}_{\mathrm{Na}^+} = 3256\,\mathrm{mS/cm^2}$; $\overline{g}_{\mathrm{K}^+} = 2200\,\mathrm{mS/cm^2}$; $\overline{g}_{\mathrm{K}^+_{\mathrm{AHP}}} = 0.15\,\mathrm{mS/cm^2}$; $\overline{g}_{\mathrm{Ca}^{2+}} = 3.7\,\mathrm{mS/cm^2}$.

### 2.5. *Synapses*

Both the full and reduced models received inputs from simulated geniculate afferents. Geniculate axons are known to be glutaminergic and access the $\alpha$-amino-3-hydroxy-5-methyl-4-isoxazoleproprionic acid (AMPA) subtype of glutamate receptor on pyramidal and stellate cells in a turtle's visual cortex [3, 17]. It was assumed that geniculate axons also access AMPA receptors on subpial cells, and the membrane equation for each compartment contained a term representing AMPAergic synapses on that compartment. The reversal potential of AMPAergic synapses was measured as +2.9 mV [3] and was assumed to be 0 mV for subpial cells. The synaptic conductance for AMPAergic synapses was given by a dual exponential function. For the full compartment model, maximal conductance and the open and close time constants, $\tau_1$ and $\tau_2$, were constrained using presumed unitary excitatory postsynaptic potentials (EPSPs) recorded from real subpial cells (Colombe, unpublished results). The EPSP with the fastest rise time was selected from a sample of EPSPs recorded in tetrodotoxin. It was assumed that this EPSP resulted from activation of a synapse on, or near, the soma of the cell. Parameters in the dual exponential function were varied until the EPSP produced by activating a synaptic current on the soma compartment of the model exactly matched the real EPSP in amplitude, rise time and half-width. Parameter values were $\overline{g}_{\mathrm{AMPA}} = 40\,\mathrm{pS}$, $\tau_1 = 1.5\,\mathrm{ms}$ and $\tau_2 = 0.5\,\mathrm{ms}$.

Geniculate axons course from lateral to medial across the visual cortex [22] and intersect the dendrites of the subpial cells [6], bearing varicosities *en passant* [22]. To provide synaptic inputs to the two versions of the full compartmental model, a fascicle of 39 geniculate axons was constructed using the image analysis system on the confocal microscope. This system allows the investigator to draw lines through an image. In this case, 39 individual lines representing geniculate axons were drawn through the image of the dendritic tree of the subpial cell. Any axon that passed

within 50 $\mu$m of the cell was assumed to affect a synapse on the cell at that point, and a synaptic conductance was included in the membrane equation of the corresponding compartment of the model. Most of the axons affected two synapses on the subpial cell. An arbitrary zero plane was defined at the lateral edge of the subpial cells, and the time required for an action potential to propagate from that plane to the compartment on which the synaptic current was placed was calculated using the conduction velocity, 0.18 $\mu$m/s, measured for geniculate afferents [7]. Geniculate neurons respond to a moving stimulus with a train of action potentials [4]. Data from the Boiko paper [4] was used to construct a sequence of action potentials in the geniculate afferents. The data set was a sequence of six action potentials at 0, 11, 107, 235, 246 and 252 ms. The spike onsets generated in individual afferents were distributed at random over a 20 ms time window so that there was a stochastic factor in the firing patterns of the afferents.

### 2.6. *Large-scale model*

The reduced compartmental model was used in a large-scale model of the turtle's visual cortex. In brief, individual neurons were assigned spatial distributions that corresponded to the anatomically determined distributions of neurons in the turtle's visual cortex (Fig. 6). Each neuron was represented as a compartmental model with 12–16 compartments based on the morphology of each type of neuron as seen in Golgi preparations. Biophysical parameters were constrained using the responses of neurons following intracellular current injections. Each neuron had a spike-generating mechanism implemented using Hodgkin-Huxley-like kinetic schemes. In addition, models of pyramidal cells had a high threshold calcium conductance and a calcium dependent potassium conductance that was responsible for spike rate adaptation in the pyramidal cells. Geniculate neurons were single compartments with a spike-generating mechanism. Two hundred and one geniculate neurons were distributed evenly along a line representing the horizontal meridian of visual space. The geniculate neurons were numbered from 1 through 201 along the the horizontal meridian from left to right. Geniculate axons were implemented as delay lines with conduction velocities constrained by the experimentally measured conduction velocities of geniculate axons.

The large-scale model used in this study is an extension of the Nenadic *et al.* [23] model. It includes 44 subpial cells, each represented by the reduced compartmental model based on cell 3-12-99, that were not included in the original model. The subpial cells were numbered arbitrarily from 1 through 44. They received geniculate inputs, inputs from pyramidal cells, and inputs from neighboring subpial cells. An AMPAergic synaptic contact was made between a geniculate afferent and each dendritic compartment of a subpial cell that was within the sphere of influence of the afferent with a radius of 25 $\mu$m. Twenty-one subpial cells had direct contacts with geniculate afferents. Of these, 16 received inputs from 1 geniculate afferent, 2 from 2 geniculate afferents, 2 from 3 geniculate afferents and 1 from 4 geniculate afferents.

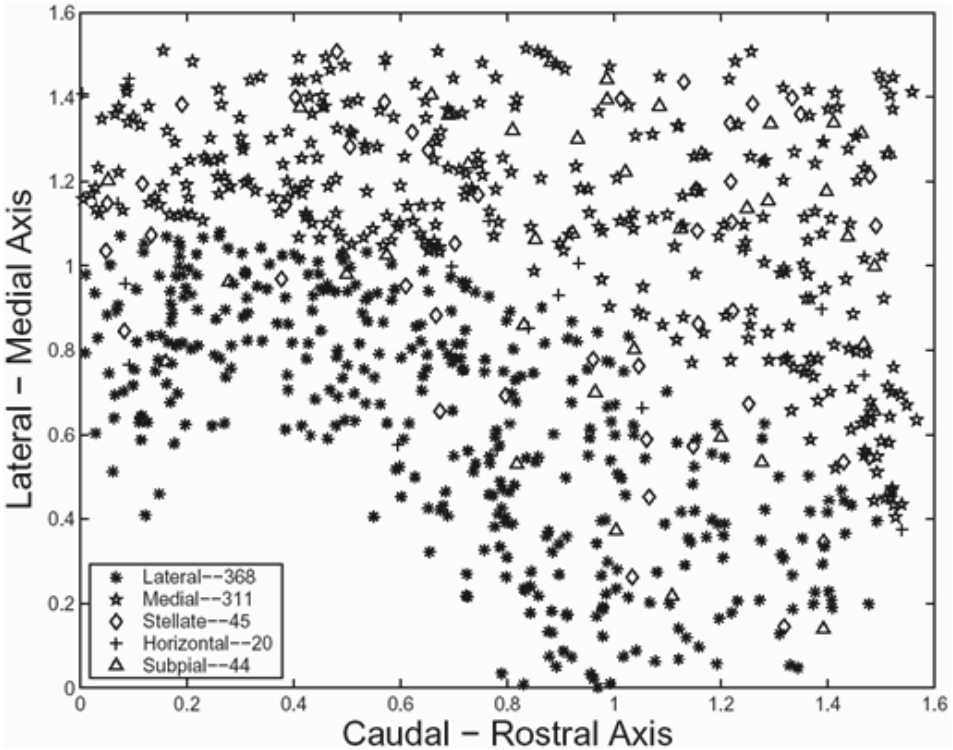


Fig. 6. Spatial distribution of model cells in the large-scale model. This figure shows the spatial distribution of lateral pyramidal, medial pyramidal, stellate, horizontal and subpial cells on an $x$, $y$ coordinate system. The numbers in the inset at the lower left indicate the number of cells of each type in the model. The dimensions of the grid are 1.6 mm on each side. Rostral is to the left. The lower edge of the coordinate system represents the lateral edge of the visual cortex.

The synapses of geniculate afferents on subpial cells were AMPAergic. They had maximal conductances of $\overline{g}_{\mathrm{AMPA}} = 5.0\,\mathrm{nS}$, and the open and close time constants of $\tau_1 = 3.0\,\mathrm{ms}$ and $\tau_2 = 0.3\,\mathrm{ms}$, respectively. Subpial cells received inputs from pyramidal cells following the same connectivity rules and synaptic kinetics described for the connections between pyramidal cells and other neurons by Nenadic *et al.* [24]. An AMPA-receptor mediated contact and an NMDA-receptor mediated contact were made between a lateral pyramidal afferent and the dendritic compartment 6 of a subpial cell that was within the sphere of influence of the afferent with a radius of 250 $\mu$m. Similarly, an AMPA-receptor mediated contact and an NMDA-receptor mediated contact was made between a medial pyramidal afferent and the dendritic compartment 16 of a subpial cell that was within the sphere of influence of the afferent with the same radius. The maximal conductance was $\overline{g}_{\mathrm{AMPA}} = \overline{g}_{\mathrm{NMDA}} = 5.0\,\mathrm{nS}$, and the open and close time constants were $\tau_1 = 3.0\,\mathrm{ms}$ and $\tau_2 = 0.3\,\mathrm{ms}$ for AMBAergic synapses and $\tau_1 = 80.0\,\mathrm{ms}$ and $\tau_2 = 0.67\,\mathrm{ms}$ for NMDAergic synapses, respectively. Subpial cells provided inhibitory inputs to pyramidal cells by effecting GABAergic synapses onto dendritic compartment 4 of lateral pyramidal cells or

dendritic compartment 2 of medial pyramidal cells within the sphere of influence of the subpial afferent with a radius of 350 $\mu$m. The synapses involved both the $GABA_A$ and $GABA_B$ subtypes of GABA receptors. They had maximal conductances of $\overline{g}_{GABA} = 5.0$ nS. Subpial cells were also connected to other subpial cells through dendritic compartment 24 of the subpial cells occurring within the sphere of influence of the subpial afferent with a radius of 350 $\mu$m. The synapses between a subpial cell and other subpial cells were GABAergic and involved both the $GABA_A$ and $GABA_B$ subtypes of GABA receptors. The maximal GABAergic synaptic conductances are $\overline{g}_{GABA} = 3.5$ nS. The open and close time constants were $\tau_1 = 1.7$ ms and $\tau_2 = 1.7$ ms for $GABA_A$ subtype of receptor mediated synapses and $\tau_1 = 500.0$ ms and $\tau_2 = 500.0$ ms for $GABA_B$ subtype of receptor mediated synapses, respectively. The kinetics of these synapses were the same as those described for GABAergic synapses by Nenadic *et al.* [24]. The spiking mechanism was located in the soma compartment of the subpial cells.

### 2.7. *Simulations*

The models were implemented using the *Genesis* software package [5] on a Dell Precision Workstation with 1 Gbyte of RAM and a 1 GHZ processor speed. Individual simulations with the full compartmental models took several minutes. Simulations with the large-scale model required about 2 hours. Diffuse retinal flashes were simulated by simultaneously injecting square current pulses of 150 ms duration into all 201 geniculate neurons. Spots of light were simulated by simultaneously injecting 150 ms current pulses into groups of 20 geniculate neurons. Moving spots were simulated by injecting current pulses into groups of geniculate neurons with various delays, beginning at different positions along the row of geniculate neurons, and moving from left to right or from right to left. Responses of the visual cortex were simulated for 1500 ms.

## 3. Results

### 3.1. *Integration of geniculate inputs by subpial cells*

Since subpial cells are embedded in the fascicle of geniculate afferents, it is likely that geniculate afferents are a dominant source of synaptic inputs to subpial cells and that geniculate synapses contact the entire dendritic arbors of individual cells. This section describes the results of simulation experiments that used the full compartmental model to examine the integration of inputs from groups of geniculate neurons by an individual subpial cell.

The effectiveness of synapses at different regions on the dendritic tree of the full compartmental model was characterized by systematically activating unitary conductances on each compartment of the model, with all of the active conductances blocked, and by measuring the amplitudes of the resulting EPSPs in the somatic

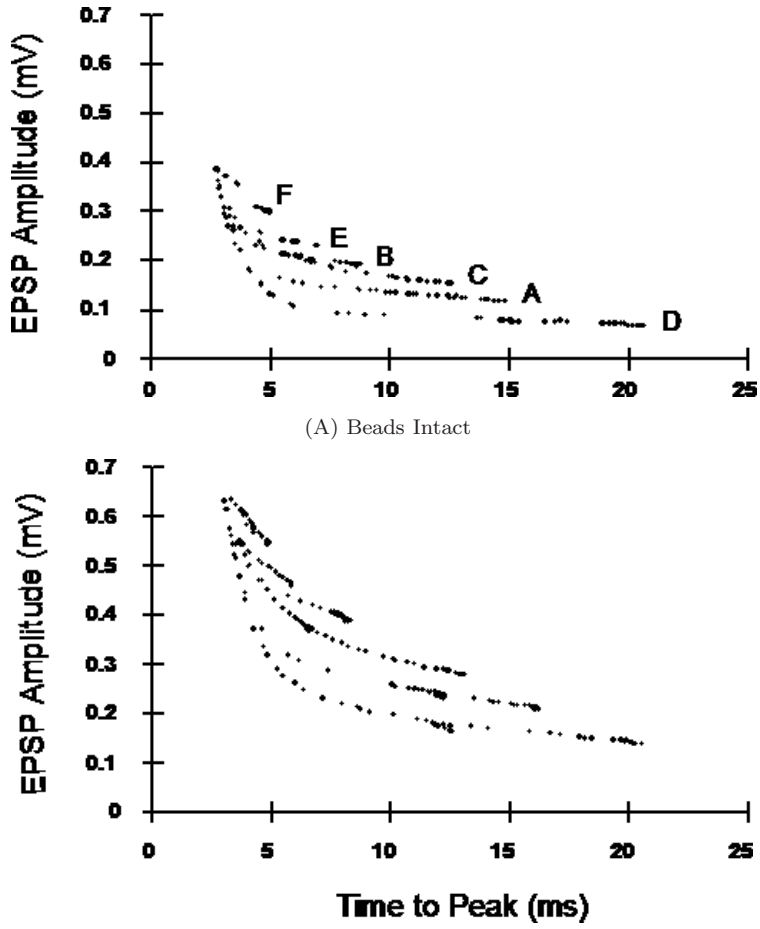


Fig. 7. Shape-index plots for passive full compartment models. These plots show the amplitudes of EPSPs generated by activation of single synapses in each soma and dendritic compartment of the two passive full compartment models and recorded in the soma compartment of the respective model. Amplitudes of EPSPs are plotted on the vertical axes. Times-to-peak of the EPSPs are plotted on the horizontal axes. EPSPs generated in each dendrite produce an arc of points in the shape index plots. The arcs resulting from primary dendrites A through F of cell 3-12-99 are indicated on the upper plot. (A) The shape index plot for the full compartment model with beads intact. (B) The shape index plot for the full compartment model with beads removed.

compartment (Fig. 7A). The most distal synapses produced EPSPs in the soma compartment that were approximately 25% of the amplitudes of EPSPs generated by activating a synaptic conductance in the soma compartment. There is, thus, a significant, electrotonic attenuation of synaptic potentials along the lengths of the dendrites, but even the most distal synapses produced EPSPs with significant amplitudes at the soma. Figure 7B shows a series of EPSPs produced by activating the same synaptic conductances with the beads removed. The amplitudes of all of the EPSPs recorded at the soma are increased, indicating that the beads on subpial

cells have the effect of decreasing the amplitudes of EPSPs generated throughout the dendritic trees of the cells, which suggests that there may be a difference in the input resistances of the two models. The responses of the full compartmental model, with beads and without beads, to intrasomatic current injections are compared in Fig. 4B. The response of the model with beads removed was a hyperpolarizing voltage transient with an amplitude 1.6 times the amplitude of the voltage transient produced in the model with beads intact. The model without beads, thus, has an input resistance of 2.3 GΩ that is 1.6 times the input resistance of the model with beads intact. The increase in the total input resistance of the passive model is due to the reduction in total surface area caused by removing the beads. Analysis of its voltage transient showed that the model with beads removed has a membrane time constant of $\tau_0 = 37.0$ ms, an equalizing time constant of $\tau_1 = 1.1$ ms. These values are essentially the same as those for the real cell and the model with beads intact. Synapses situated on the dendrites of the model with beads removed thus produce larger EPSPs in the soma compartment than synapses on the dendrites of the model with beads intact do. These results follow from the basic biophysics of neurons. The time constants depend upon the specific resistance and capacitance of the membrane, but not on the total surface area of the cell.

Individual axons course from lateral to medial across the dendritic arbors of subpial cells, bearing varicosities on average at intervals of 16 $\mu$m [22]. The conduction velocity of geniculate afferents in the turtle visual cortex has been measured at 0.18 $\mu$m/$\mu$s, so it will take an action potential approximately 88 $\mu$s to travel between two successive varicosities on a geniculate afferent and 1.1 ms to cross the approximately 200 $\mu$m that span the dendritic arbor of cell 3-12-99. Activation of a bundle of geniculate afferents results in a series of EPSPs generated on different compartments of different dendrites in a 36 ms time window. This situation was examined in a simulation experiment, using a bundle of 39 geniculate afferents constructed with the image analysis system of the confocal microscope as described in the Methods section above. Activation of a single axon resulted in EPSPs in one or more compartments of the subpial cell. The timing of successive EPSPs (if the axon made more than one contact on the cell) was determined by the propagation time between the two synaptic sites. Consequently, we carried out a series of simulations using realistic spike trains in the geniculate afferents in models with spike generating mechanisms. The number of geniculate axons activated was systematically increased from 1 through 39. Activation of various combinations of 1 through 37 axons in the model with beads intact resulted in complex sequences of EPSPs that remained below threshold and did not generate an action potential. Activation of 38 axons resulted in a single action potential (Fig. 8A). By contrast, an action potential could be generated in the model with beads removed by activation of only 12 geniculate axons (Fig. 8B). Activation of 38 axons generated four action potentials (Fig. 8B). These simulations indicate that the beads on the dendrites of subpial cells significantly decrease the numbers of action potentials generated in subpial cells by realistic trains of EPSPs in geniculate axons.

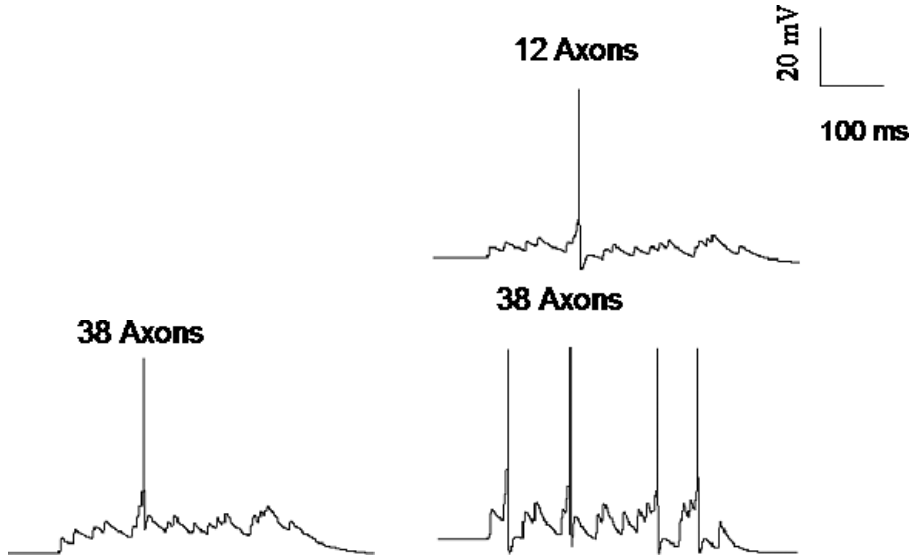


Fig. 8. Responses of model cells with active conductances to the asynchronous activation of geniculate afferents. (A) An action potential produced in the full compartmental model with active conductances by activation of 38 geniculate axons when beads are intact. Activation of fewer than 38 axons did not produce an action potential. (B) Activation of 12 axons produced a single action potential in the full compartmental model when beads are removed. Activation of 38 geniculate afferents produced multiple action potentials.

### 3.2. *Responses of subpial cells to simulated diffuse light flashes*

Figure 9A shows the response of the large-scale model to a simulated diffuse retinal flash in the form of a space-time plot. The firing pattern of each cell is represented by a row of dots, each dot representing the occurrence of an individual action potential. Responses of each type of cell are positioned together. Responses of subpial cells are shown at the top of the plot, followed by horizontal cells, stellate cells, medial pyramidal cells, and finally lateral pyramidal cells. Responses of individual cells of a given type are ordered according to their approximate positions along the rostral-caudal axis of the cortex. The subpial cells fire in a strong burst of action potentials between 20 ms and about 180 ms. Their activity then declines, but increases again between about 330 ms and 950 ms. This pattern is shown in more detail in Fig. 10A, which plots the spike occurrences of only the 44 subpial cells in the large scale model. It is clear that in this plot not all of the individual subpial cells fire in response to the simulated flash, and that individual cells do not necessarily fire in both the initial and late components of the response. The initial component involves 21 of the 44 subpial cells, and consists of a train of action potentials in the first 200 ms following stimulus onset. The second component involves 22 of the subpial cells with action potentials distributed between 200 ms and 1000 ms following stimulus onset.

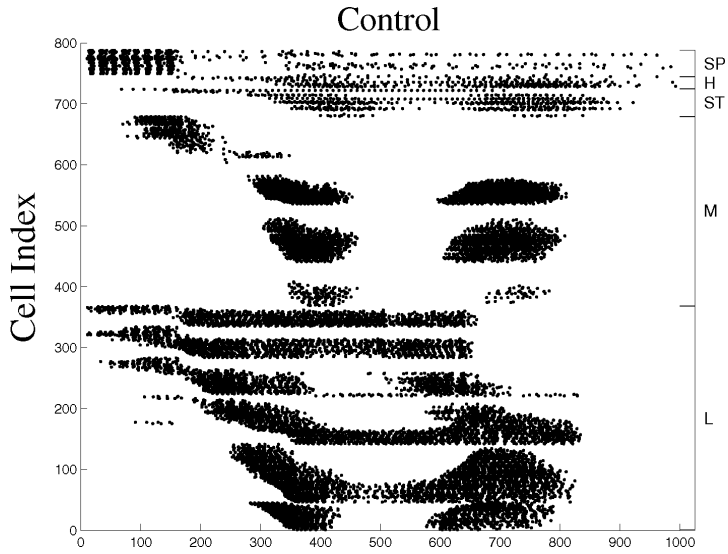


(A)

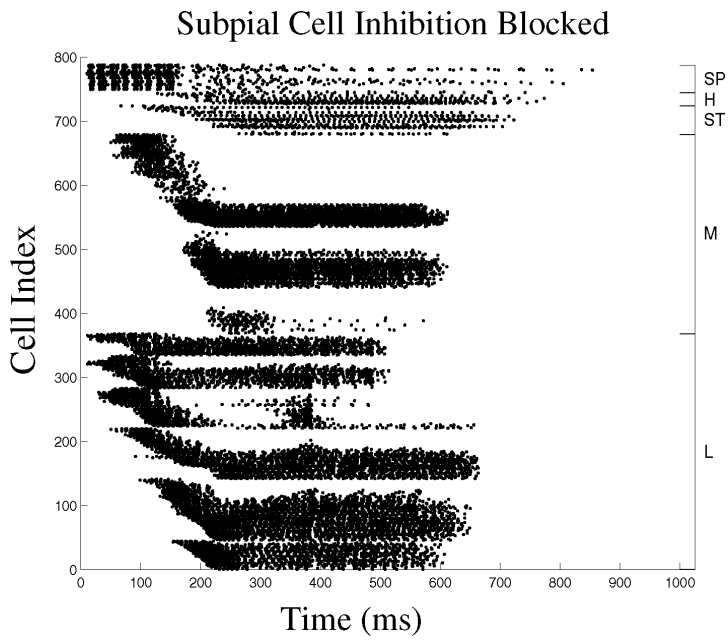


(B)

Fig. 9. Responses of subpial cells to simulated diffuse light flashes. Responses of the model to simulated diffuse light flashes are represented as space-time plots. The firing pattern of each cell in the model is represented as a row of dots; each dot represents the time of occurrence of an action potential in that cell. Firing patterns of subpial cells are represented at the top of the figure, followed by those of horizontal cells, stellate cells, medial pyramidal cells and lateral pyramidal cells. Individual cells within each group are ordered by their approximate positions along the rostral-caudal axis of the model, so that their firing latencies are an index of the progression of the wave across the cortex. (A) Response of the model with all synaptic interactions intact. (B) Response of the model with the synapses of subpial cells on other neurons blocked.

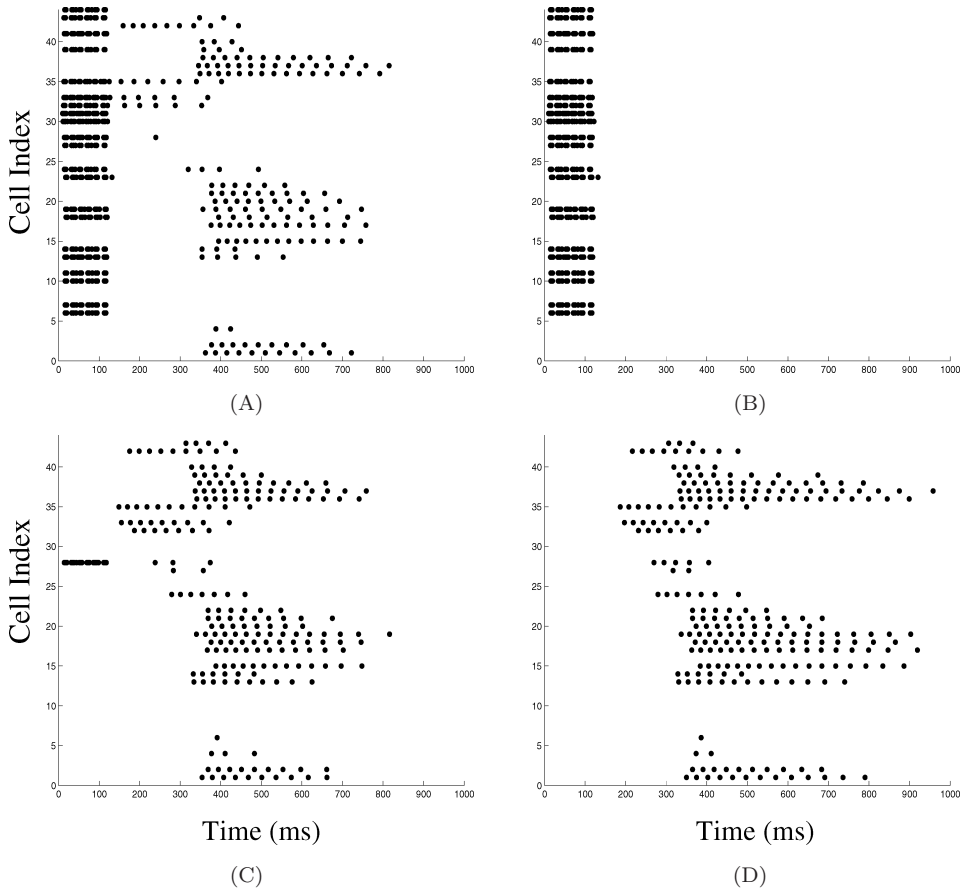


Fig. 10. Firing patterns of subpial cells. This figure shows the firing patterns of the 44 subpial cells in the large-scale model. The vertical axis in each plot is an index of the individual subpial cells. The horizontal axis represents time after stimulus presentation. Thus, the bottom horizontal line of dots shows the firing times of subpial cell 1; the top horizontal line of dots shows the firing times of subpial cell 44. (A) Responses of the 44 subpial cells to a diffused light flash, simulated by simultaneously activating all 201 geniculate neurons for 150 ms. (B) Responses of the 44 subpial cells with all recurrent excitation from pyramidal cell collaterals blocked. (C) Responses of the 44 subpial cells to simultaneous activation of geniculate neurons 1–20 and 61–80. (D) Responses of the 44 subpial cells to simultaneous activation of geniculate neurons 1–20 and 21–40.

To study the contributions of geniculate and pyramidal cell afferents to the firing patterns of subpial cells, we first simulated the response to a diffuse retinal flash with the recurrent excitation of pyramidal cells on subpial cells blocked by setting the synaptic conductances from pyramidal cells to subpial cells as zero (Fig. 10B). Only the fast component of the response occurs, demonstrating that it is due to direct geniculate input while the slow phase is due to recurrent excitation. We then studied the contributions of the geniculate inputs to the variation seen in the firing patterns of individual subpial cells by simulating the responses of subpial cells to two disjunct spots of light flashed simultaneously for 150 ms. Figure 10C shows the response of

the subpial cells to activation of geniculate neurons 1–20 and neurons 61–80. Cell number 28 fires action potentials in the fast component of the response and then between 220 ms and 400 ms after stimulus onset in the slow component. This cell received direct inputs from geniculate neurons 71 and 74. Twenty-five other subpial cells responded during the slow component of the response. Figure 10D shows the responses of the subpial cells to activation of geniculate neurons 1–20 and 21–40. None of the subpial cells receive direct inputs from these two groups of geniculate neurons. Consequently, none of the subpial cells fire during the fast component of the response but many fire during the slow component. This occurs because geniculate inputs synapse directly on pyramidal cells and generate a wave of activity that propagates across the cortex from its rostral pole to its caudal pole. There is, in general, a significant variation in the onset of the slow component of the response between different subpial cells that reflect the dynamics of the wave propagating across the cortex, because cells situated near the rostral pole of the cortex fire relatively early while cells near the caudal pole of the cortex fire later.

### 3.3. *Responses of subpial cells to simulated apparent motion stimuli*

Mazurskaya [21] studied the responses of her superficial units to two spots of light presented at different points in visual space with a range of temporal delays. We simulated these experiments by injecting 60 ms current pulses in two clusters of 25 geniculate neurons each (neurons 82–106 and 108–132) with a range of interstimulus intervals (Fig. 11). Figure 11A shows the response of all of the cells in the model to simultaneous activation of the two spots as a space-time plot. The firing patterns of the subpial cells generally resemble those evoked by a simulated diffuse flash in that they have fast and slow components. Figures 11B and 11C show the responses to clusters of geniculate neurons activated with delays of 100 ms and 120 ms, respectively. The firing patterns of subpial cells in these cases resemble the results obtained by Mazurskaya in that there are three distinct components. The first two are relatively fast components that result from the activation of the two groups of geniculate neurons. The third is a slow and prolonged component that results from the recurrent excitation of the subpial cells by the pyramidal cells. This can be seen in the space-time plots by comparing the onset of pyramidal cell firing to the onset of the slow component of subpial cell firing.

### 3.4. *Responses of subpial cells to simulated moving stimuli*

Figure 12 shows the firing patterns of subpial cells in response to simulated moving stimuli. These cases involve varying both the spatial and temporal patterns of geniculate afferents. Spots moving from left to right (or from right to left) were simulated by injecting current pulses of 150 ms duration into 6 groups of 20 geniculate neurons each with various delays. Figures 12A and 12B show the responses of the subpial cells to activation of geniculate neurons by spots moving from left to right

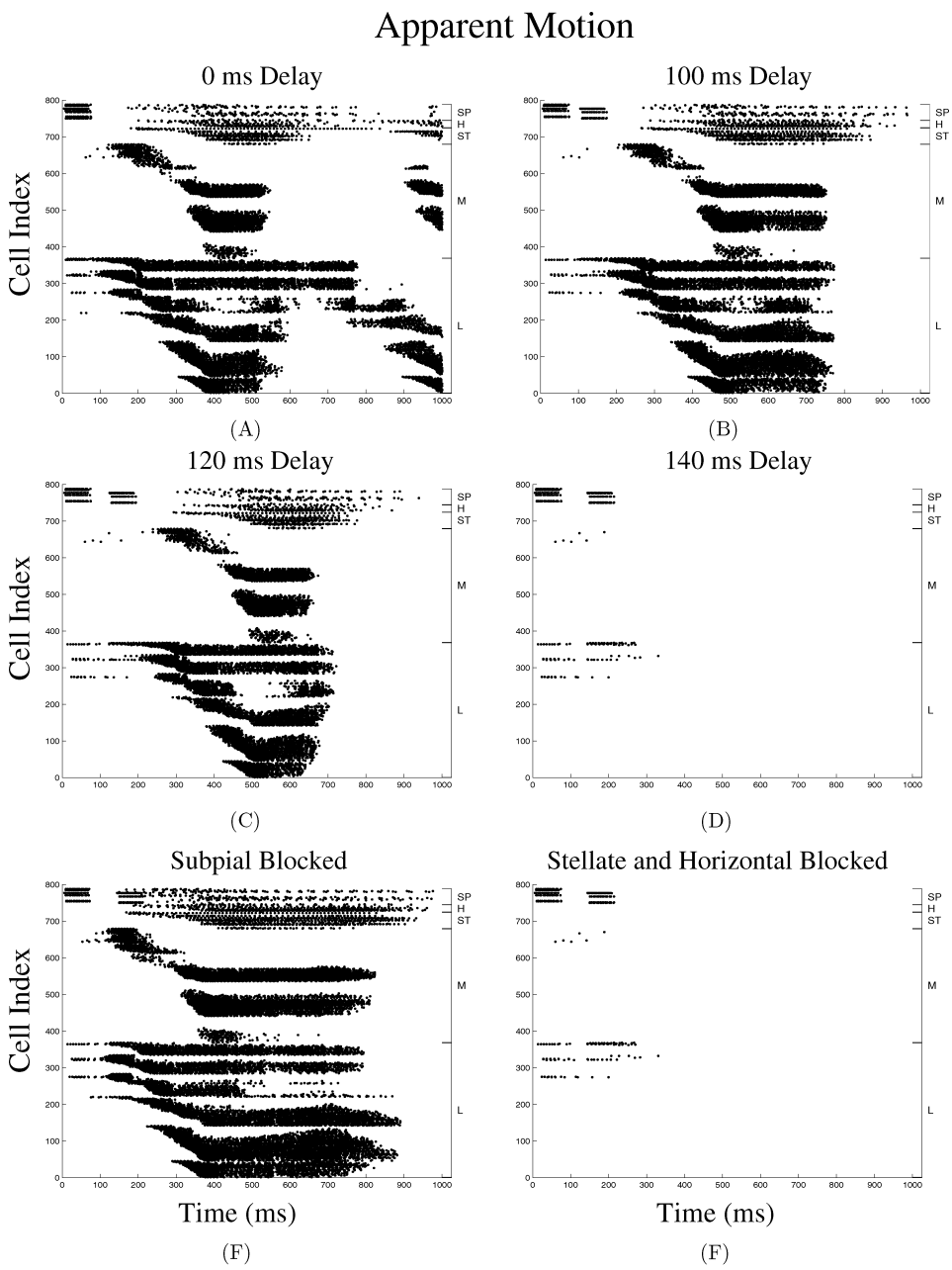


Fig. 11. Responses of subpial cells to simulated apparent motion stimuli. Response of the large scale model to activation of two groups of 25 geniculate neurons each with a range of delays between the onset of the first and second groups. The first group consisted of neurons 82–106; the second group consisted of neurons 108–132. (A) Simultaneous activation of the two groups of neurons (that is, a delay of 0 ms). (B) Activation of the two groups of neurons with a delay of 100 ms. (C) Activation of the two groups of neurons with a delay of 120 ms. (D) Activation of the two groups of neurons with a delay of 140 ms. (E) Activation of the two groups of neurons with a delay of 140 ms and the inhibition from subpial cells to other cells in the cortex blocked. (F) Activation of the two groups of neurons with a delay of 140 ms and the inhibition from stellate and horizontal cells to other cells in the cortex blocked.

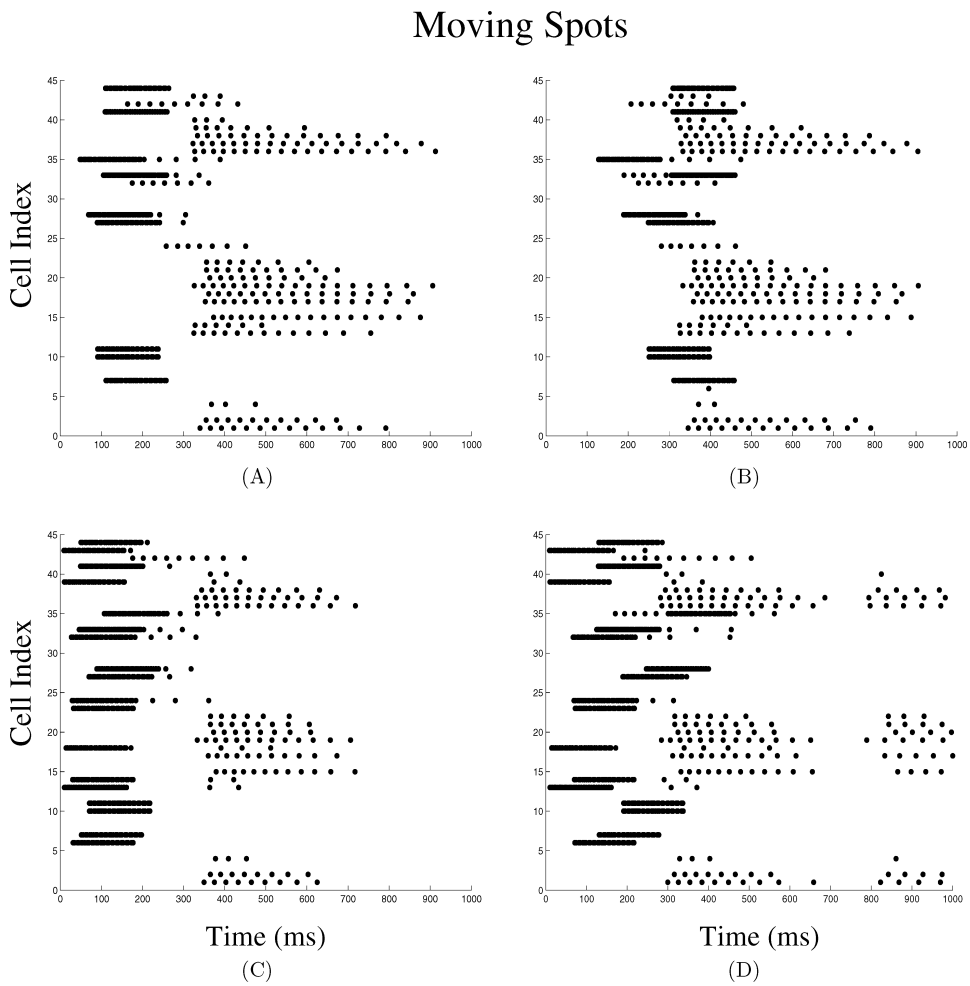


Fig. 12. Responses of subpial cells to simulated moving stimuli. Responses of the subpial cells in the large scale model to four different stimuli moving either from left to right or from right to left with delays of 20 ms and 60 ms, respectively. The 6 groups of geniculate neurons in the case of stimuli moving from left to right were neurons 1–20, 21–40, 41–60, 61–80, 81–100 and 101–120 along the row of geniculate neurons. The 6 groups of geniculate neurons in the case of stimuli moving from right to left were neurons 141–160, 121–140, 101–120, 81–100, 61–80 and 41–60. Each space-time plot shows the firing pattern of all of the subpial cells to sequential activation of a sequence of geniculate neurons. (A) Responses of the subpial cells to a stimulus moving from left to right with delays of 20 ms. (B) Responses of the subpial cells to a stimulus moving from left to right with delays of 60 ms. (C) Responses of the subpial cells to a stimulus moving from right to left with delays of 20 ms. (D) Responses of the subpial cells to a stimulus moving from right to left with delays of 60 ms.

with delays of 20 ms and 60 ms, respectively, between the onset of current injections. The six groups of geniculate neurons activated by moving spots were neurons 1–20, 21–40, 41–60, 61–80, 81–100 and 101–120 along the row of geniculate neurons. Figures 12C and 12D show the responses of the subpial cells to activation of geniculate neurons by moving spots from right to left with delays of 20 ms and 60 ms,

respectively. The six groups of geniculate neurons activated by moving spots were neurons 141–160, 121–140, 101–120, 81–100, 61–80 and 41–60. All four of the cases that are illustrated show the fast phase of subpial cell firing resulting from the activation of geniculate afferents, and the slow phase resulting from the recurrent excitatory drive produced by the primary and secondary propagating waves. However, there are detailed differences in which individual subpial cells are activated in the latencies and durations of their action potential trains. The comparison of Figs. 12A and 12B or Figs. 12C and 12D indicates that moving spots with different delays or, equivalently, different speeds, produce differences in the timing of the fast phase of subpial cell firing, although the same subset of subpial cells are activated in the same order in each case. Similar variations are visible in 26 additional simulations that were carried out with a range of stimulus conditions.

### 3.5. *Effects of subpial cell inhibition on pyramidal cells*

The firing patterns of the lateral and medial pyramidal cells show three components (Fig. 9A) that have been described by Wang *et al.* [37]. An initial burst of activity occurs in the rostral pole of the cortex in the two groups of pyramidal cells between 20 ms and 150 ms. This corresponds to an initial depolarization that is seen in activity plots of simulation experiments [37] and in the real cortex in voltage sensitive dye experiments. The second component is a primary propagating wave that begins at about 150 ms in the lateral pyramidal cells and somewhat later in the medial pyramidal cells. The activity of both lateral and medial pyramidal cells ceases between 450 ms and 600 ms, but builds up again at about between 600 ms and 800 ms. This secondary wave is propagating from caudal to rostral across the cortex. A notable feature of Fig. 9A is that the generation of the primary propagating wave in the lateral pyramidal cells occurs at about 150 ms as the firing frequency of the subpial cells is decreasing. Since the subpial cells are inhibitory, this suggests that the generation of the primary propagating wave is controlled by the level of the activity of the subpial cells. This is demonstrated explicitly in the experiment illustrated in Fig. 9B. It shows the response of the large-scale model to the same simulated stimulus, except that the inhibitory synapses of the subpial cells on pyramidal cells were blocked. The latencies of both the lateral and medial pyramidal cells are now reduced and the slope of the latencies of the lateral pyramidal cells is increased. This simulation demonstrates that subpial cells firing in the first phase control the latency and speed of the primary propagating waves.

The two responses in Figs. 11B and 11C also show a progressive delay in the onset and a shortening of the duration of the primary propagating wave and complete inhibition of the secondary propagating wave. Figure 11D shows the response to activating the two clusters of geniculate neurons with a delay of 140 ms. Activation of the second cluster in this case occurs when the primary propagating wave is forming and inhibits its formation. The response, thus, shows only the two clusters of action potentials produced in the subpial and lateral pyramidal cells by activity

in the geniculate afferents. Figures 11E and 11F show the responses to activating the two clusters of geniculate neurons with the same delay as for the simulation depicted in Fig. 11D. However, the inhibition from subpial cells (Fig. 11E) or from stellate and horizontal cells (Fig. 11F) was blocked. A propagating wave was produced when inhibition from subpial cells to all other cells in the cortex was blocked, but not when inhibition from stellate and horizontal cells to all other cells in the cortex was blocked. These simulations involve activating the same sets of subpial cells with different temporal relations and demonstrate that the timing of firing in different populations of subpial cells can strongly influence the dynamics of the primary and secondary propagating waves.

## 4. Discussion

### 4.1. *Are superficial units the same as subpial cells?*

A central assumption in this study is that the cells that Mazurskaya [21] identified as superficial units using extracellular recording methods in alert turtles correspond to the anatomically defined subpial cells that have been studied by Desan [9] and by Colombe *et al.* [6]. This assumption could, in principle, be tested directly by repeating Mazurskaya's work using intracellular recording methods and filling the cells after they had been characterized physiologically. However, this is a relatively difficult experiment that has not been achieved to date because subpial cells are a numerically small population of neurons that are distributed sparsely in the cortex. Obtaining intracellular recordings using blind recording methods *in vivo* is, thus, very difficult. The receptive field properties of neurons in the visual cortex could, in principle, be studied using an eye-brain *in vitro* preparation (see Mancilla *et al.* [9]), but it is also difficult to locate subpial cell in this preparation. The best results in studying subpial cells [6] were obtained using infrared differential interference contrast optics and a slice preparation, which does not permit characterizing receptive field properties because the retinogeniculate projection is interrupted in preparing the slice. The simulation results in this study support a correspondence between superficial units and subpial cells in that the principal features of the receptive fields of superficial units could be reproduced in the large-scale model.

### 4.2. *Limitations of the detailed model of subpial cells and the large-scale model of the cortex*

The full compartmental model of a subpial cell is based on a detailed reconstruction of the anatomy and of the intracellular physiology of cell 3-12-99 from the study by Colombe *et al.* [6]. It was one of two cells in the study in which both the somata and dendrites appeared to be completely filled. These two cells had the highest total input resistances of the 12 cells in the sample, suggesting that they were the results of the best penetrations obtained in the study. Otherwise, the anatomy and physiology of cell 3-12-99 were generally consistent with those of the other cells in

the sample. The relationship of geniculate afferents to subpial cells is an important feature of this study, so care was taken to use detailed anatomical information on the size and distribution of subpial cells [6] and the geometry and distribution of varicosities on geniculate afferents [22]. The principal gap in our knowledge of subpial cells is in characterizing their voltage-gated conductances. General kinetic schemes for sodium, potassium and calcium conductances were used in this study. The kinetic parameters were constrained by comparing the responses of the model cell to simulated depolarizing current pulses to the responses of the real cell to intracellular current injections. It was possible to accurately reproduce the initial phase of the firing pattern of the real cell in the model cell using this approach. The incorporation of a calcium-dependent potassium conductance in the model cell caused it to show a distinct spike rate adaptation that is characteristic of subpial cells [23]. Since the detailed kinetics of the calcium-dependent conductances and of the cell's intracellular calcium buffering mechanisms are not known, it was not possible to accurately reproduce the timing of spikes in the late phase of the cell's firing pattern. Including a mechanism to produce spike-rate adaptation in the model is important because this feature distinguishes subpial cells from the other two major populations of inhibitory interneurons in the visual cortex (stellate and horizontal cells), which show little spike rate adaptation. However, the simulations carried out in this study did not depend upon the detailed firing patterns of the subpial cells and it is unlikely that the variations seen in the timing of individual spikes in the late firing phase of subpial cells has any affect on the conclusions of the study.

The experimental data used to construct the large-scale model of visual cortex are discussed in some detail by Nenadic *et al.* [23] and Wang *et al.* [37]. In brief, the distribution of neurons in the model is based upon the known spatial distribution of neurons in turtle visual cortex. As in the case of subpial cells, the compartmental models that represented the other classes of cells in the cortex are based upon relatively good information on the anatomy, physiology and synaptology of the cells, but only generic features of their firing patterns are reproduced in the individual models because of a lack of information on the kinetics of the voltage-gated conductances of the real cells. However, care has been taken to incorporate a mechanism for spike rate adaptation in the models representing those classes of cells that show spike rate adaptation. The models, thus, capture the basic distinction between regular spiking and fast spiking cells, but not the detailed firing patterns of individual cells. The principal limitation of the model from the perspective of the current study is that the spatial distribution of subpial cells in the model is based on the spatial distribution of cells in the outer layer 1 of the cortex. This distribution was based on the distribution of neurons in sections through a cortex stained for Nissl substance with cresyl violet. Subpial cells cannot be distinguished in such preparations from the other classes of cells present in layer 1, and no specific markers for subpial cells are known at this time. Deviations from the actual distribution of subpial cells would produce detailed variations in the direction and speed of propagating waves in the

model. However, these deviations cannot be sufficiently large to change the results reported here, which depend upon the general timing of the primary and secondary propagating waves. These features of the model are entirely consistent with data obtained with voltage sensitive dye methods [23, 30].

### 4.3. *Subpial cells have wide receptive fields*

Mazurskaya [21] found that superficial units respond to moving bars or small spots of light presented anywhere in binocular visual space. However, the dendritic arbors of subpial cells have widths only 10%–30% the length of visual cortex [6]. It is now known that the projection of the retina on the dorsal lateral geniculate complex is topographically organized with the nasal-temporal axis of the retina represented along the rostral-caudal axis of the geniculate and the dorsal-ventral axis of the retina represented along the ventral-dorsal axis of the geniculate [36]. Geniculate axons run from the cortex to the lateral edge of the visual cortex and then course across the cortex bearing varicosities *en passant* [22]. Each fascicle of geniculate axons carries information from a specific eccentricity along the horizontal meridian of visual space. Cortical neurons form bands, or isoazimuth lamellae, that extend across the lateral-medial edge of the cortex. Neurons within a given isoazimuth lamella receive inputs from geniculate afferents carrying information from a restricted range along the horizontal meridian of visual space. An apparent paradox, then, is how subpial cells can have wide receptive fields given that their dendritic arbors span only a fraction of the length of the visual cortex.

The same problem pertains to subpial cells in our large-scale model, which receive direct geniculate inputs from only a fraction of the total number of geniculate afferents so that a considerable fraction of subpial cells in the model are not directly activated by geniculate inputs. However, our large-scale model does not include a retina and geniculate neurons are activated by intracellular current injections. Real geniculate neurons receive convergent inputs from many retinal ganglion cells and have receptive fields that range from 10° to 40° in diameter [4, 21]. Convergence of several geniculate afferents on a subpial cell would, thus, produce a receptive field with a diameter of at least 40°. Consistent with this, Mazurskaya's data suggest that individual subpial cells can integrate information from geniculate neurons that respond to 1° loci in visual space separated by up to at least 60°. Convergence of inputs from geniculate neurons positioned at several different points along the rostral-caudal axis of the geniculate would result in even larger receptive fields, but the degree of convergence is probably not sufficient to account for the formation of receptive fields that encompass all of binocular visual space. Our simulations suggest that subpial cells can be brought to threshold by visual stimuli presented at any point in visual space because such stimuli always produce a wave of activity that propagates across the cortex. Those subpial cells in the large-scale model that do not receive direct retinal inputs are still activated indirectly by geniculate afferents that trigger a propagating wave. The wide field receptive fields of subpial cells

would, then, result from a combination of direct geniculate inputs and pyramidal cell inputs. This hypothesis can be tested in future *in vivo* experiments by quantitative characterization of the receptive fields of superficial units. The simulation results suggest that the receptive field would have a central region that fires robustly and with short latency in response to the presentation of small spots of light in a relatively restricted region of visual space and a large surround region that responds less strongly and with variable latency to stimuli presented at all points in visual space.

### 4.4. *Subpial cells fire in two phases*

Mazurskaya [21] studied the responses of neurons in the visual cortex of alert turtles to two spots of light presented with a range of spatial and temporal separations. Plots of the number of action potentials produced as a function of the temporal separation of the spots showed three peaks for her superficial units. Our simulations of the responses of subpial cells to diffuse flashes to two spots of light, and to moving spots indicate that subpial cells fire in two phases. A fast phase consists of a burst of action potentials triggered by activation of geniculate neurons. The slow phase consists of a prolonged and less intense train of action potentials caused by the primary and secondary waves propagating across the cortex and activating subpial cells via their recurrent collaterals. The occurrence of the fast and slow phases in the response of the cortex depends upon the stimulus used to evoke the response. Responses to diffuse stimuli have two components because all of the geniculate afferents are activated simultaneously. The response, thus, shows an early component that corresponds to the fast phase caused by simultaneous activation of all of the geniculate afferents and a late component that corresponds to the slow phase caused by pyramidal cell excitation to the subpial cells. Stimuli consisting of two spots of light produce responses that have three components. The first two components result from activation of two groups of geniculate neurons; the third results from the propagating wave. A difference between our simulation results and Mazurskaya's experimental results is that the time between the first and second peaks in Mazurskaya's plots is longer than the time between the first two firing components in our simulations. However, our model does not account for the time required for photoreceptor activation, intraretinal processing and the conduction of action potentials from the retina to the geniculate. Assuming that the latency for responses to the second spot is on the order of 150 ms [15, 19], the first two components in our simulations would have a temporal separation comparable to that seen between the two peaks in Mazurskaya's data.

### 4.5. *Subpial cell activation leads the activation of pyramidal cells*

Mazurskaya [21] showed plots of action potentials produced by two spots of light as a function of the temporal separation of the spots for both superficial and deep units. The deep units undoubtedly correspond to pyramidal cells, which comprise the substantial majority of cells in layer 2. Plots for the superficial and deep units differ

in that the superficial units show a short latency peak that is not seen in the plots for deep units. This suggests that the latency to spike production is much shorter in superficial units than it is in deep units. Our large-scale simulations are entirely consistent with this experimental finding in that subpial cells fire well in advance of pyramidal cells. Both sets of findings are also consistent with intracellular recording experiments using the *in vitro* eye-brain preparation and diffuse retinal flashes (Mancilla *et al.* [21]). EPSPs recorded from layer 2 regular spiking cells, which are presumed to be pyramidal cells, have latencies in the range of 157.8 ms to 220.8 ms following light onset [21]. The latency for the production of action potentials was $639 \pm 64$ ms. By contrast, the latencies for EPSPs in presumed inhibitory interneurons were in the range of 109.0 ms–137.3 ms and the latency for the production of action potentials was $280 \pm 35$ ms.

There appear to be several factors that favor the production of action potentials with relatively short latencies in subpial cells. The first is that the subpial cells are literally embedded in the fascicle of geniculate afferents, so each subpial cell is likely to be postsynaptic to a large number of geniculocortical synapses. Quantitative studies (Curtis and Ulinski, unpublished observations) of the lateral geniculate complex in turtles indicate it contains approximately 13,000 neurons. Although there is some controversy on the issue of whether or not all geniculate neurons project to the cortex [14], it does appear that the cell plate neurons [26] that comprise about 92% of neurons in the complex do project to the cortex. The axons of geniculate neurons course across the visual cortex with relatively little branching. Assuming that roughly 13,000 geniculate axons are distributed across the rostral-caudal axis of the visual cortex and that the visual cortex is about 2000 $\mu$m in length, then a subpial cell with a dendritic arbor 210 $\mu$m in width would intersect roughly 1400 geniculate axons. Smith *et al.* [32] used electron microscopic methods to estimate that cells with smooth dendrites received approximately 1800 synaptic contacts from thalamic axons. They referred to the cells they studied as "stellate cells", but restricted their sample of degenerating terminals to the outer 100 $\mu$m of the cortex. It is, thus, likely that the majority of the smooth (i.e., non-spiny) dendrites included in their sample were from subpial cells. The large thalamic lesions they used included non-specific thalamic nuclei that project to the visual cortex as well as the lateral geniculate complex [12, 38], so it is reasonable to use 1400 as a rough estimate of the number of geniculate synapses on one subpial cell. Simulations with our full compartmental model suggest that simultaneous activation of 38 geniculate neurons is sufficient to generate a single spike in a subpial cell. The rough calculations outlined above, thus, suggest that each subpial cell receives synaptic contacts from many more geniculate axons than are required to bring the cell to its firing threshold, so a relatively weak visual stimulus would be adequate to fire a subpial cell. Consistent with this, Mancilla *et al.* [19] found that cortical neurons have thresholds of about only 100 photons/$\mu$m/s following diffuse light flashes.

A series of biophysical properties also contribute to the relative sensitivity of subpial cells to geniculate activation. Subpial cells have significantly higher input

resistances ($723 \pm 109\,\mathrm{M}\Omega$ versus $131 \pm 14\,\mathrm{M}\Omega$) and significantly shorter membrane time constants ($45.5 \pm 5.2$ ms versus $140 \pm 62$ ms) than do pyramidal cells [6, 8, 19]. Subpial cells have mean electrotonic lengths of $1.1 \pm 0.2$ [6] and EPSPs generated in distal dendritic compartments of our full compartmental model have amplitudes that are about 25% of those generated in the proximal dendritic or soma compartments. The electrotonic length of a subpial cell is, thus, sufficiently small for EPSPs generated in even the distal dendrites to contribute to spike generation in the soma compartment of the model.

There is a basic tradeoff between a neuron's sensitivity to its inputs and its ability to integrate information from multiple inputs. A subpial cell, that is sufficiently sensitive to geniculate inputs could be brought to threshold and fire strongly in response to activation of a single geniculate afferent. It would, then, be difficult for such a cell to integrate inputs from many geniculate afferents. Simulations in which the beads were removed from our full compartmental model show that the beads tend to decrease the sensitivity of the cell, so that a greater number of geniculate afferents are required to bring a cell with beads intact to its firing threshold than if the beads are removed. A larger number of action potentials are produced by a given input in model cells without dendritic beads than in cells with the beads intact. It is possible that the beads, thus, increase the ability of the cell to integrate inputs from disjunct regions of visual space. Because subpial cells are embedded in the band of geniculate inputs, they will receive strong excitation whenever a cluster of geniculate neurons is active. This insures that subpial cells will fire reliably in the first phase of their firing pattern. However, this sensitivity makes it likely that a stimulus occurring in a restricted region of visual space has a high probability of causing the cell to fire. The dendritic beads may increase the probability of stimuli from two or more regions of visual space to fire the cell.

Dendritic beads are a common feature of interneurons in mammalian visual cortex. Dendritic beads or varicosities are seen frequently in illustrations of non-pyramidal neurons (e.g., [1, 11, 18]). Cells with varicose dendrites are often identified as either axoaxonic or basket cells ([1, 25]). The results presented in this paper appear to be the first discussion of a potential function for dendritic beads. Removing the beads in our model of a subpial cell changes the surface area of the cell and increases its input resistance. The same changes would be caused by deleting the beads from dendrites of basket or of axoaxonic cells. It is possible that reducing the sensitivity of interneurons to multiple inputs is a general design strategy in cortical microcircuits.

### 4.6. *Function of subpial cells*

Our simulations suggest that the inhibition of pyramidal cells by subpial cells is important in controlling the firing patterns of pyramidal cells. Blocking inhibition of pyramidal cells by subpial cells in simulations of diffuse light flashes decreases the latency of pyramidal cell firing and increases the intensity of pyramidal cell firing

in both the initial depolarization and propagating waves of the cortical responses. Simulations of apparent motion stimuli indicate that presenting the second spot of light controls the latency of the pyramidal cell response, and that a spot presented during the transition from the initial depolarization to the primary propagating wave can prevent formation of the wave. Simulations of moving spots indicate that spots moving in different directions and with different speeds can produce distinct spatiotemporal patterns in the subpial cell population.

Subpial cells could, thus, regulate the activation of pyramidal cells in both of their firing phases. Direct activation of subpial cells by geniculate afferents may be timed so that it can control the rising phases of EPSPs in pyramidal cells, while the activation of subpial cells by recurrent excitation can control the falling phases of EPSPs in pyramidal cells. Mancilla and Ulinski [20] recorded from presumed pyramidal cells with electrodes filled with the $GABA_A$ receptor antagonist, picrotoxin. They found that blockade of $GABA_A$ receptor mediated inhibition to the cell being recorded, and increased the slopes of the rising phases of EPSPs induced by electrical activation of geniculate afferents. In addition, picrotoxin increased the amplitudes of the falling phases of light and induced EPSPs. Visual stimuli would be expected to produce a brief but strong inhibition of pyramidal cells, followed by a longer phase of mild inhibition.

Several studies in our laboratories have now shown that waves in both the real visual cortex of turtles and in our large scale model contain information about the positions and speeds of visual stimuli [10, 23, 29]. Du *et al.* [10] found that the probability of making an error in detecting the positions of stimuli in visual space decreased linearly in probability during the first 200 ms of the simulated wave. Since this is the time during which the initial depolarization is being formed and undergoing a transition to the propagating wave, it appears that the cortical response has the greatest information content during this time period. Wang *et al.* [37] used the large scale model to show that the synaptic strengths between the different populations of excitatory and inhibitory cells in the large scale model can control the formation, speed, and duration of the waves. It is, thus, reasonable to hypothesize that synaptic strength could be a major factor controlling the information content of the waves. However, Wang *et al.* [37] examined the effects of varying synaptic strengths on the discriminability of stimuli and found that synaptic strengths do not have a major effect. By contrast, the simulations in this paper suggest that different visual stimuli would activate the population of subpial cells in rather different spatiotemporal patterns during both firing phases. There are, in particular, distinct spatiotemporal patterns during the fast firing phase when the information content of the responses appears to be greatest. Since the subpial cells fire in advance of the pyramidal cells during this phase and inhibit them, the spatiotemporal firing pattern of the subpial cells may determine which pyramidal cells fire as the wave is forming and shape the dynamics of the initial depolarization in this way.

**Acknowledgments**

This work was supported by grants from the Learning in Intelligent Systems and Collaborative Research in Computational Neuroscience from the National Science Foundation to B. K. Ghosh and P. S. Ulinski. Ulinski was also supported by the Faculty Research fund at the University of Chicago.

**References**

[1] Asouz R, Gray CM, Nowak LG, McCormick DA, Physiological properties of inhibitory interneurons in cat striate cortex, *Cereb Cortex* **7**:1047–3211, 1997.

[2] Blanton MG, Kriegstein AR, Properties of amino acid neurotransmitter receptors of embryonic cortical neurons when activated by exogenous and endogenous agonists, *J Neurophys* **67**:1185–1200, 1992.

[3] Blanton MG, Shen JM, Kriegstein AR, Evidence for the inhibitory neurotransmitter $\gamma$-aminobutyric acid in aspiny and sparsely spiny nonpyramidal neurons of the turtle dorsal cortex, *J Comp Neurol* **259**:277–297, 1987.

[4] Boiko VP, Responses to visual stimuli in thalamic neurons of the turtle, *Emys orbicularis, Neurosci Behav Physiol* **10**:183–188, 1980.

[5] Bower JM, Beeman D, *The Book of Genesis*, 2nd ed., TELOS, New York, 1998.

[6] Colombe JB, Sylvester J, Block J, Ulinski PS, Subpial and stellate cells: Two populations of interneurons in turtle visual cortex, *J Comp Neurol* **471**:333–351, 2004.

[7] Colombe JB, Ulinski PS, Temporal dispersion windows in cortical neurons, *J Comput Neurosci* **7**:71–87, 1999.

[8] Connors BW, Kriegstein AR, Cellular physiology of the turtle visual cortex: Distinctive properties of pyramidal and stellate neurons, *J Neurosci* **6**:164–177, 1986.

[9] Desan PH, The organization of the cerebral cortex of the pond turtle, *Pseudemys scripta elegans*. Ph.D. Thesis, Harvard University, Cambridge, MA, 1984.

[10] Du X, Ghosh BK, Ulinski PS, Encoding and decoding target locations with waves in the turtle visual cortex, *IEEE Trans Biomed Eng* **52**:566–577, 2005.

[11] Freund TF, Martin KAC, Smith AD, Somogyi P, Glutamate decarboxylase-immunoreactive terminals of Golgi-impregnated axoaxonic cells and of presumed basket cells in synaptic contact with pyramidal neurons of the cat's visual cortex, *J Comp Neurol* **221**:263–278, 1983.

[12] Hall JA, Foster RE, Ebner FF, Hall WC, Visual cortex in a reptile, the turtle (*Pseudemys scripta* and *Chrysemys picta*), *Brain Res* **130**:197–216, 1997.

[13] Heller SB, Ulinski PS, Morphology of geniculocortical axons in turtles of the genera *Pseudemys* and *Chrysemys*, *Anat Embryol* **175**:505–515, 1987.

[14] Kenigfest NB, Repérant J, Rio J-P, Belekhova MG, Tumoanova NL, Ward R, Veselkin NP, Herbin M, Chkeidze DD, Ozirskaya EV, Fine structure of the dorsal lateral geniculate nucleus of the turtle, *Emys orbicularis*. A Golgi, combined HRP tracing and GABA immunochemical study, *J Comp Neurol* **356**:595–614, 1995.

[15] Kriegstein AR, Synaptic responses of cortical pyramidal neurons to light stimulation in the isolated turtle visual system, *J Neurosci* **7**:2488–2492, 1987.

[16] Kriegstein AR, Connors BW, Cellular physiology of the turtle visual cortex: Synaptic properties and intrinsic circuitry, *J Neurosci* **6**:178–191, 1986.

[17] Larson-Prior LJ, Ulinski PS, Slater NT, Excitatory amino acid receptor-mediated transmission in geniculocortical and intracortical pathways within visual cortex, *J Neurophysiol* **66**:293–306, 1991.

[18] Lund JS, Organization of neurons in the visual cortex, area 17, of the monkey (*Macaca mulatta*), *J Comp Neurol* **147**:455–496, 1973.

[19] Mancilla JG, Fowler M, Ulinski PS, Responses of regular spiking and fast spiking cells in turtle visual cortex to light flashes, *Vis Neurosci* **15**:979–993, 1998.

[20] Mancilla JG, Ulinski PS, Role of $GABA_A$-mediated inhibition in controlling the responses of regular spiking cells in turtle visual cortex, *Vis Neurosci* **18**:9–24, 2001.

[21] Mazurskaya PZ, Study of the projection of the retina to the forebrain of the tortoise *Emys orbicularis*, *J Evol Biochem Physiol* **8**:550–555, 1972.

[22] Mulligan KA, Ulinski PS, Organization of geniculocortical projections in turtles: Isoazimuth lamellae in the visual cortex, *J Comp Neurol* **296**:531–547, 1990.

[23] Nenadic Z, Ghosh BK, Ulinski PS, Modelling and estimation problems in the turtle visual cortex, *IEEE Trans Biomed Eng* **49**:753–762, 2002.

[24] Nenadic Z, Ghosh BK, Ulinski PS, Propagating waves in visual cortex: A large-scale model of turtle visual cortex. *J Comput Neurosci* **14**:161–184, 2003.

[25] Palwelzik H, Hughes DI, Thomson AM, Physiological and morphological diversity of immunocytochemically defined parvalbumin- and cholecystokinin-positive interneurones in CA1 of the adult rat hippocampus, *J Comp Neurol* **443**:346–367, 2002.

[26] Rainey WT, Ulinski PS, Morphology of neurons in the dorsal lateral geniculate complex in turtles of the genera *Pseudemys* and *Chrysemys*, *J Comp Neurol* **253**:440–465, 1986.

[27] Rall W, Time constants and electrotonic length of membrane cylinders and neurons, *Biophys J* **9**:1483–1508, 1969.

[28] Reiner A, A comparison of neurotransmitter-specific and neuropeptide-specific neuronal cell types present in the dorsal cortex in turtles with those present in the isocortex in mammals: Implications for the evolution of isocortex, *Brain Behav Evol* **38**:53–91, 1991.

[29] Robbins KA, Senseman DM, Extracting wave structure from biological data with application to responses in turtle visual cortex, *J Comput Neurosci* **16**:267–298, 2004.

[30] Senseman DM, Spatiotemporal structure of depolarization spread in cortical pyramidal cell populations evoked by diffuse retinal light flashes, *Vis Neurosci* **16**:65–79, 1999.

[31] Senseman DM, Robbins KA, High-speed VSD imaging of visually evoked cortical waves: Decomposition into intra- and intercortical wave motions, *J Neurophysiol* **87**:1499–1514, 2002.

[32] Smith LM, Ebner FF, Colonnier M, The thalamocortical projection in *Pseudemys* turtles: A quantitative electron microscope study, *J Comp Neurol* **190**:445–461, 1980.

[33] Stratford K, Mason A, Larkman A, Major G, Jack JJB, The modeling of pyramidal neurons in the visual cortex, in Durbin R, Miall C, Mitchison G (eds.), *The Computing Neuron*, Addison-Wesley, Workingham, pp. 296–321, 1989.

[34] Ulinski PS, Organization of corticogeniculate projections in the turtle, *Pseudmys scripta, J Comp Neurol* **254**:529–542, 1986.

[35] Ulinski PS, Neural mechanisms underlying the analysis of moving stimuli, in Ulinski PS, Jones EG, Peters A (eds.), *Cerebral Cortex, Vol. 13. Models of Cortical Circuitry*, Plenum Press, New York, pp. 283–399, 1999.

[36] Ulinski PS, Nautiyal J, Organization of retinogeniculate projections in turtles of the genera *Pseudemys* and *Chrysemys*, *J Comp Neurol* **276**:92–112, 1988.

[37] Wang W, Campaigne C, Ghosh BK, Ulinski PS, Two cortical circuits control propagating waves in visual cortex, *J Comput Neurosci* **19**:263–289, 2005.

[38] Zhu D, Lustig LH, Bifulco K, Keifer J, Thalamocortical connections in the pond turtle *Pseudemys scripta elegans*, *Brain Behav Evol* **65**:278–292, 2005.